World Academy of Science, Engineering and Technology
International Journal of Electronics and Communication Engineering
Vol:19, No:6, 2025

Multisource Radio Frequency and Solar Energy Harvester for Internet of Things

Emmanuel Ekwueme, Anwar Ali, Saeed Ur Rehman

Abstract**—**As the Internet of Things (IoT) continues to expand, the demand for battery-free devices is increasing, which is crucial for the efficiency of 5G networks and eco-friendly industrial systems. The solution is a device that operates indefinitely, requires no maintenance, and has no negative impact on the ambient environment. One promising approach to achieve this is energy harvesting, which involves capturing energy from the ambient environment and transferring it to power devices. This method can revolutionize industries; such as manufacturing, agriculture, and healthcare by enabling real-time data collection and analysis, reducing maintenance costs, improving efficiency, and contributing to a future with lower carbon emissions. This research explores various energy harvesting techniques, focusing on radio frequencies (RF) and multiple energy sources. It examines RF-based and solar methods for powering battery-free sensors, low-power circuits, and IoT devices. The study investigates a hybrid RF-solar harvesting circuit designed for remote sensing devices. The proposed system includes distinct RF and solar energy harvester circuits, with the RF harvester operating at 2.45 GHz and the solar harvester utilizing a maximum power point tracking (MPPT) algorithm to maximize efficiency.

Keywords**—**Radio frequency, energy harvesting, Internet of Things, IoT, multisource, solar energy.

I. Introduction

THE challenge in using wireless sensor networks (WSN) and the IoT is battery replacement. Given the large number of WSN or IoT devices, some of which are hard to reach, changing batteries is often impractical or too time-consuming. To overcome this difficulty, scientists have proposed several ambient energy harvesting (EH) strategies [1]. A variety of energy sources, including vibration [2], heat [3], light [4], and electromagnetic (EM) RF waves, have been proposed as means of capturing energy in a variety of scenarios [5]. Nevertheless, the reliability of the obtained power is diminished by these ambient sources' erratic and inconsistent nature. Mixed energy harvesters, such as combining solar and RF [6], solar and vibration [7], or solar, vibration, and piezoelectric sources [8], have been proposed to mitigate this. Because of its widely available sources, RFEH (Radio Frequency Energy Harvesting) is the most favorable. On the other hand, because inside locations have intense lighting, solar EH can produce significant output power. Thus, combining solar and RFEH systems into a hybrid RF-solar energy harvester is a workable alternative that delivers energy diversity.

A. Challenges and Limitations of Energy Harvesting

EH, while promising, faces a number of obstacles: low energy density; variable availability of ambient energy sources; requirement for highly efficient energy conversion systems; for instance, solar energy is not available at night, and radiofrequency energy is highly location-dependent; additionally, the energy harvested from these sources is typically relatively small (microwatts to milliwatts), which restricts the categories of powered devices.

- *Limited Life and Frequent Battery Replacements:* One major drawback of IoT devices is the short lifespan of standard batteries. Particularly in high-energy gadgets, batteries deteriorate over time and should be changed periodically. Replacing or recharging thousands or millions of batteries is impractical and expensive in large-scale IoT installations, such as smart cities or industrial environments. These also lead to longer device outages, which interfere with vital functions [9].
- *Environmental Impact and Sustainability Issues:* The increasing use of traditional batteries affects the environment because of electronic waste (e-waste). Batteries contain harmful materials like lead, mercury, and cadmium, which can damage the environment when not disposed of correctly. Additionally, mining for the raw materials used to make batteries can harm the environment [10].
- *Energy Inefficiency:* Because they lose power during conversion, self-discharge, and are sensitive to temperature changes, traditional power sources —especially batteries— become less and less effective with time. Energy management is a major difficulty for long-term operation of IoT devices because of this inefficiency, which can lead to decreased performance or early battery failures [11].
- *Maintenance and Operational Costs:* IoT devices that rely on traditional batteries face high operational costs because of the ongoing maintenance required, such as battery replacement and device servicing. In large-scale IoT deployments, this results in substantial labor and financial expenses, diminishing the overall cost-effectiveness of these systems [12].
- *Scalability Issues:* Traditional power sources restrict the scalability of IoT systems. Regular battery replacements and the logistical challenges of managing numerous devices with limited power capacity hinder the efficient scaling of IoT networks. Powering thousands or millions of

Emmanuel Ekwueme and Anwar Ali are with Department of Electronic and Electrical Engineering, Swansea University, UK (e-mail: anwar.ali@swansea.ac.uk).

Saeed Ur Rehman is with Faculty of Science and Engineering, University of Hull, Hull, UK.

devices with traditional sources is unsustainable in large deployments, such as smart cities or industrial monitoring [13].

B. Importance of Multisource Energy Harvesting

Multisource EH, which involves capturing energy from various environmental sources, is gaining significant importance across numerous technological fields. Integrating diverse energy sources such as solar, RF, thermal, and mechanical energy offers a more dependable, efficient, and sustainable power supply for low-power devices. This approach is crucial for the growing use of IoT devices, WSN, wearable electronics, and remote sensing applications. These technologies all require a steady and uninterrupted power source [14].

- *Improved Power Supply Reliability and Continuity:* This is one of the main advantages of multisource EH. Every energy source has limitations, such as the erratic nature of RF waves or the sporadic nature of solar energy. These shortcomings can be lessened by combining many energy-gathering techniques. For example, solar energy is unavailable at night or under cloudy conditions, while RF energy can be continuously collected at a lower power. Integrating various energy sources produces a more reliable and continuous power supply, which is important for critical applications such as environmental monitoring, industrial automation, and healthcare [15].
- Energy Efficiency Optimization: Multisource EH optimizes available ambient energy, increasing energy efficiency. Traditional single-source energy harvesters are limited by the availability and sufficiency of their specific energy source. An EH system can improve overall energy collection by dynamically selecting the most efficient energy source at any given time by mixing different sources, such as solar and RF. Adaptive energy switching circuits and MPPT are examples of advanced power management systems that may optimize energy extraction from each source in response to current conditions [16].
- *Lower Upkeep and Operational Expenses:* One notable benefit of multisource EH is decreased upkeep and running expenses linked to battery-operated equipment. Sensors in industrial equipment and other devices placed in difficult-to-reach or remote areas frequently depend on batteries that need to be changed or recharged regularly, which raises the cost of operation. Multisource EH, which offers a steady and sustained energy supply from ambient sources, can lessen the need for battery replacement. This lowers maintenance costs by enabling equipment to operate independently for extended periods [17].
- *Sustainability and Advantages for the Environment:* The environmental impact of electronic systems and sustainability are significantly affected by multisource EH. When traditional batteries reach the end of their life cycle, hazardous chemicals and raw materials are sourced and disposed of, which adds to environmental degradation. Using renewable energy sources such as solar and radiofrequency, multisource EH lessens the dependency on batteries and the environmental consequences of battery manufacturing, use, and disposal [18].
- *Enabling Future Technologies and Innovations:* As IoT and intelligent technologies are growing in demand, self-powered devices can operate autonomously in diverse environments. Multisource EH enables future innovations by providing a reliable, scalable, and sustainable power source for these emerging technologies. For example, multisource energy harvesters in wearable electronics can capture both body heat (thermal energy) and ambient RF signals, providing a continuous power source for health monitoring devices or fitness trackers without frequent charging [19].

II. Design Specifications for RF Energy Harvesting Circuit

A. Antenna Design for 2.45 GHz

Fig. 1 illustrates a rectangular microstrip patch element placed on top of a larger rectangular ground plane, with the substrate material separating the patch element and the ground plane [20].

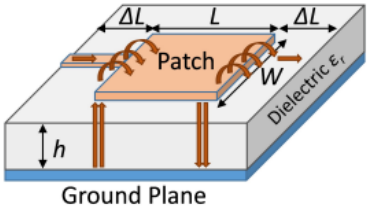

Fig. 1 Microstrip patch antenna design [20]

The rectangular microstrip antenna dimensions are determined by the width (W), length (L), height (h), and the dielectric constant (ε_r) of the substrate. Typically, the dielectric constant ranges between 2.2 and 12 [21]. The substrate selection is crucial for achieving optimal performance and the right patch element size for the microstrip patch element [22]. A lower dielectric constant and thick substrate result in better performance, high efficiency, and a larger bandwidth but also lead to an increase in patch size and, therefore, the overall antenna size.

Conversely, microwave circuitry can benefit from a higher dielectric constant and a thinner substrate because they provide close-bound fields that reduce unwanted radiation and coupling. This can result in a smaller antenna, but the efficiency is lost because of generated losses and a narrower bandwidth.

B. Design and Calculation of Parameters for Microstrip Patch Antenna

The microstrip patch antenna's width (W) and length (L) are calculated with the formulas below [23]:

Width of the patch (W):

$$W = \frac{\lambda_0}{2}\left(\frac{2}{E_r+1}\right)^{1/2} \quad (1)$$

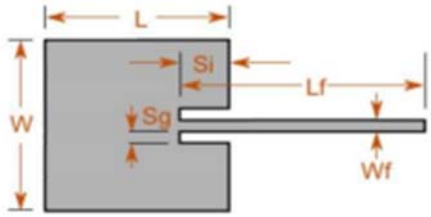

Fig. 2 Inset feed design [23]

Length of the patch (L):

$$L = \frac{1}{2fr\sqrt{\varepsilon_{eff}}\sqrt{\mu_0\epsilon_0}} - 2\Delta L \quad (2)$$

Inset length (ΔL):

$$\Delta L = 0.412h\frac{(\varepsilon_{eff}+0.3)}{(\varepsilon_{eff}-0.258)}\frac{(\frac{W}{h}+0.264)}{(\frac{W}{h}+0.813)} \quad (3)$$

Effective dielectric constant (ε_{eff}):

$$\varepsilon_{eff} = \frac{\varepsilon_r+1}{2} + \frac{\varepsilon_r-1}{2}\left(1+\frac{12h}{w}\right)^{-\frac{1}{2}} \quad (4)$$

The inset determines the antenna's impedance matching. A good value was obtained for the inset through a parameter sweep.

Table I shows the computation's outcome for the Microstrip patch antenna design parameters. Table II shows antenna's feedlines and inset parameters.

TABLE I
PARAMETERS OF MICROSTRIP PATCH ANTENNA

Parameter	Value	Units
Operating Frequency (f_0)	2.45 GHz	Hz
Ground plane dimension (L x W)	60 mm x 60 mm	mm
Patch Length (L)	29.16 mm	mm
Patch Width (W)	37.61 mm	mm
Dielectric Constant (ε_r)	4.3	-
Dielectric Material	FR-4	-
Dielectric Substrate Height (H)	1.6 mm	mm

TABLE II
PARAMETERS OF FEEDLINE AND INSET

Parameter	Value	Units
Feed Line Length (L_f)	16.94	mm
Feed Line Width (W_f)	3.11	mm
Space between feed line and patch (S_g)	6.445	mm
Feed inset from edge (S_i)	5.00	mm

C. Single-Band RF-to-DC Signal Converter Circuit At 2.45 GHz

The RF voltage multiplier/rectifier converter is essential in the RFEH system. It converts the AC RF signal received by the antenna into a steady DC signal. Since ambient RF signals usually have low power, a voltage multiplier circuit is needed to rectify the AC voltage to DC and enhance the voltage gain.

Different voltage multipliers exist, such as Cockcroft Walton, Dickson, Mandal-Sarpeshkar, and Villard circuits [24]. This paper uses the Dickson voltage multiplier circuit to convert RF to DC power, maximizing DC output for WSN sensors and other low-power applications. Fig. 3 shows a single-stage RF voltage doubler rectifier circuit with two capacitors and two diodes.

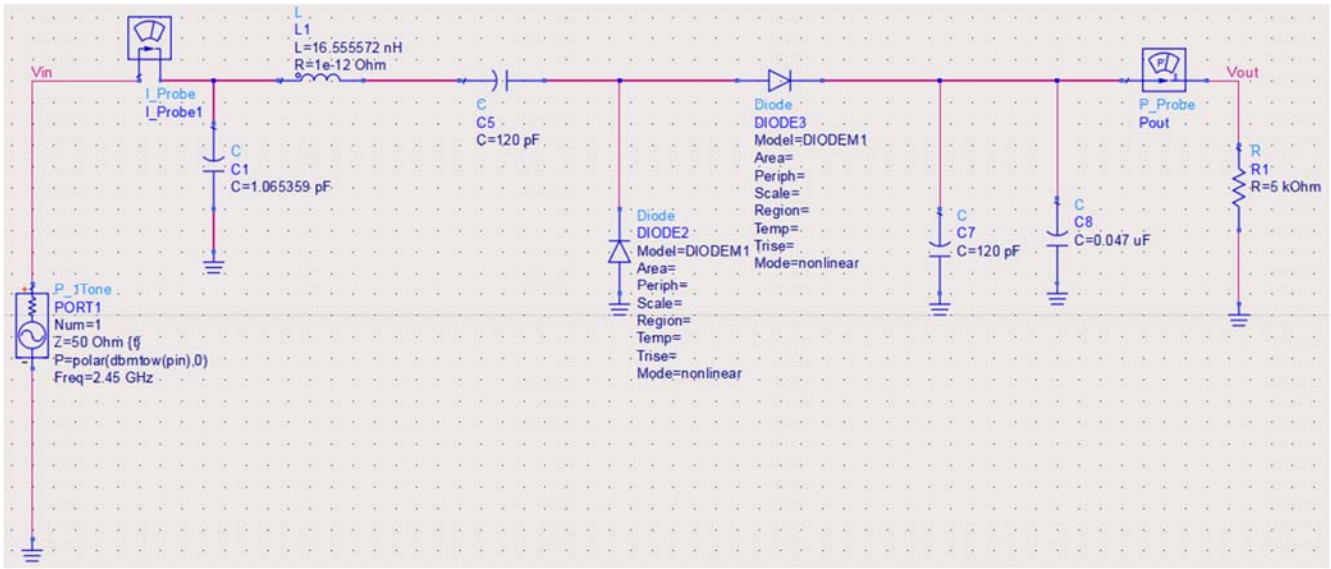

Fig. 3 Single-stage RF energy harvester for 2.45 GHz

The SMS-7630 Schottky diode is used in the voltage multiplier circuit because of its high switching speed and low cutoff voltage, making it practical for rectifying low-power high-frequency signals. The RFEH circuit was designed and simulated using Advanced Design System (ADS) simulation software from Agilent Technologies. The diode's modeling parameters are series resistance (Rs = 20 Ω), zero bias capacitance (C_{j0} = 0.14 pF), reverse breakdown voltage (B_V = 2

V), saturation current (Is = 5 × 10^{-6} A), current at reverse breakdown voltage (IBB = 1 × 10^{-4}), and emission coefficient (N = 1.05) [25].

The capacitor values were carefully chosen in the RFEH system. A high capacitance value can result in a low output AC voltage from a single stage. In contrast, a low capacitance value can cause a voltage drop during switching, leading to an improper rectifier function. The capacitor value that maximizes rectifier efficiency in this circuit is 120 nF.

The RF input signal is rectified in both positive and negative half cycles. However, the voltage across the input capacitor (C_5) in one-half cycle is transferred to the output capacitor (C_7) in the next half cycle. Thus, the output capacitor's voltage is twice the RF source's peak voltage minus the diode's turn-on voltage.

The rectifier circuit was first simulated without matching networks to determine the input impedance at 2.45 GHz. Fig. 4 shows the Smith Chart plot of the simulation results, and the input impedance at 2 and also displays the return loss coefficient.

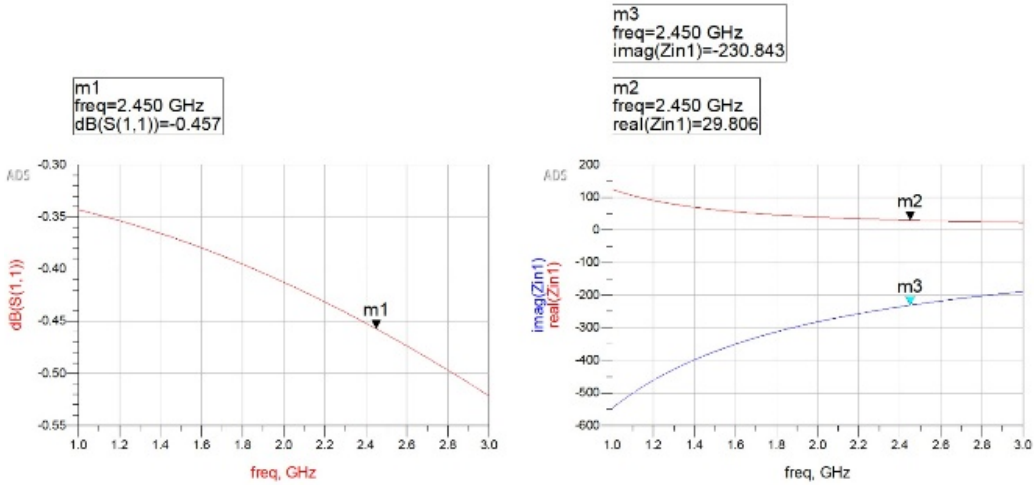

Fig. 4 The return loss coefficient and the impedance of the network without IMN

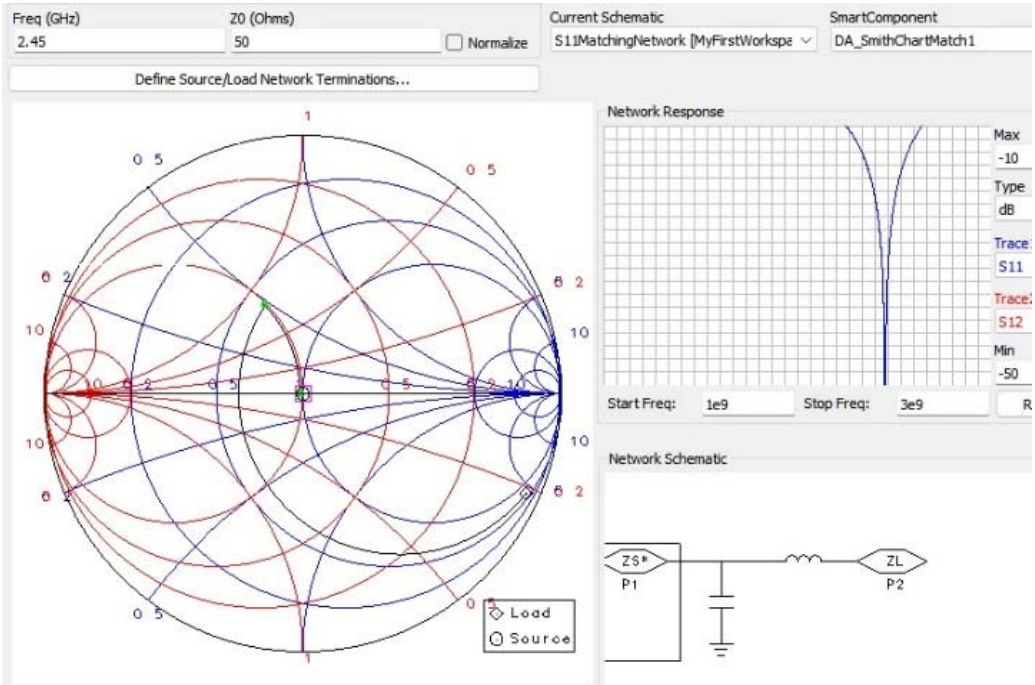

Fig. 5 Using capacitor and inductor to implement IMN in ADS

In ADS, the Smith Chart utility's rectangular plot matches the complex load impedance (Z_L) of 29.806 - j230.843 Ω at 2.45 GHz to the 50 Ω input impedance of the antenna port. The antenna port impedance is consistently set at 50 Ω during the simulation. Thus, each matching network is designed to convert the rectifier's complex input impedance to this 50 Ω antenna impedance, optimal for minimizing transmission line losses and maximizing power in SMA coaxial cables commonly used in

the communication industry [26].

D. Designing the Impedance Matching Network

RFEH systems have two Impedance Matching Network (IMN) arrangements: lumped component-based (using an inductor and a capacitor), as shown in Fig. 5 and distributed component-based (utilizing a transmission line). For this paper, a lumped component-based network was selected to match the impedances between the receiving antenna and the Voltage Multiplier Circuit (VMC).

Insertion and return loss of the IMN are critical for the RFEH system as they affect the circuit's overall efficiency. The IMN, consisting of a parallel inductor and a shunt capacitor, transforms the complex impedance of the voltage multiplier to 50 Ω.

The lumped component is added between the receiving antenna and the VMC to reduce reflected power and improve RF system effectiveness at the target frequency, ensuring maximum power transfer from the source to the load. Using the ADS Smith Chart Utility tool (Fig. 5), the lumped component IMN was designed to match the standard input antenna impedance (Zs = 50 Ω) with Z_L = 29.806 - j230.843 Ω at 2.45 GHz. Z_L represents the real and imaginary parts of the impedance, as the VMC includes a frequency-dependent capacitor.

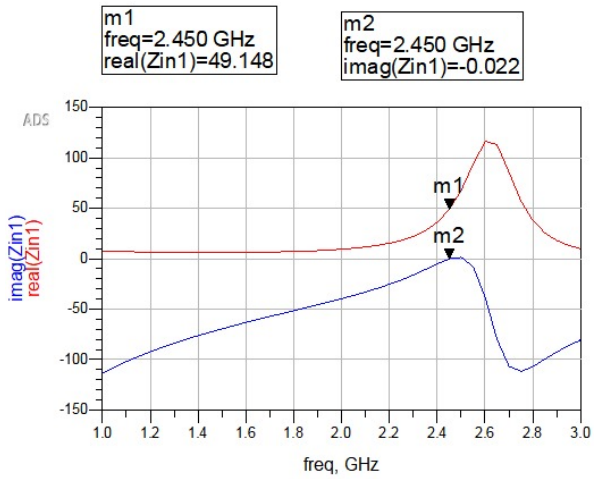

Fig. 6 The real and imaginary part of the circuit after implementing IMN

To achieve impedance matching at 2.45 GHz, the extracted optimized values from ADS are C1 = 1.065359 pF and L1 = 16.555572 nH, respectively. With the matching network, the rectifier's equivalent impedance becomes (49.913 - j0.024) Ω, which is very close to the 50 Ω input antenna port impedance. Fig. 6 shows the natural and imaginary components of Z_{in}. The simulated return loss coefficient (S_{11}) at the IMN input, shown in Fig. 7, indicates that matching at the desired frequency has been achieved.

Fig. 7 shows a graph of the reflection coefficient (S_{11}) vs. frequency to analyze the rectifier's return-loss performance with and without an impedance-matching circuit. Due to the impedance matching, the return loss significantly decreases at the matching frequency. The matching network is considered satisfactory at an input power of -30 dBm. S_{11} is -41.313 dB, as shown in Fig. 7.

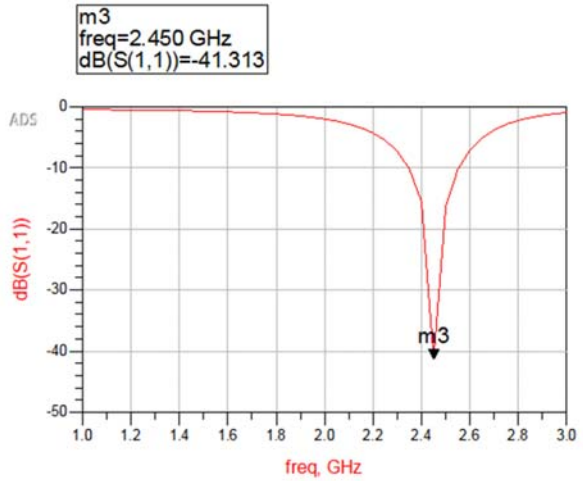

Fig. 7 The return loss coefficient after implementation of IMN

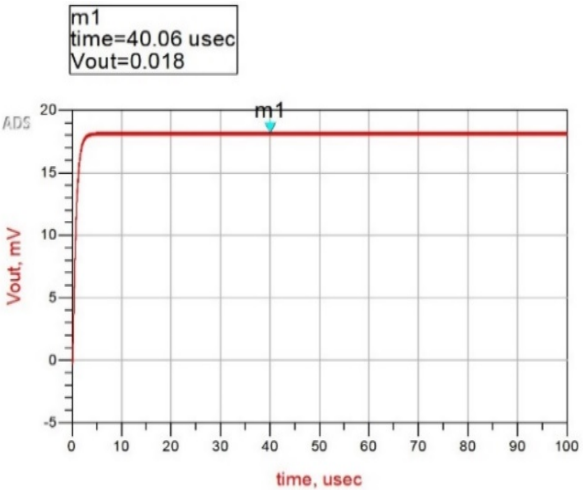

Fig. 8 (a) Design without DC pass filter for P_{in} = -30 dBm

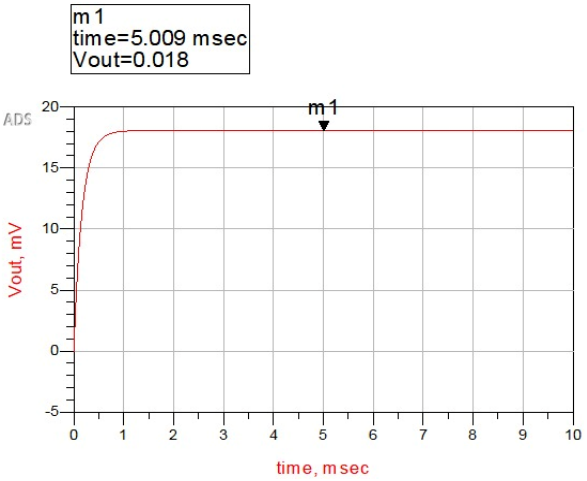

Fig. 8 (b) Design with DC pass filter for P_{in} = -30dBm

A capacitor (C8 = 0.047 µF) is used as a DC pass filter after the rectifier circuit with the matching network. This filter eliminates the harmonics produced by the diodes' nonlinear behavior and the fundamental frequency signal, as shown in Fig. 8. Smoothing the DC output voltage improves power transfer efficiency.

E. Dual-Band RF-to-DC Signal Converter Circuit at 2.45 GHz and 5.5 GHz with One Matching Network

Fig. 9 shows the circuit design for dual-band RFEH for 2.45 GHz and 5.5 GHz.

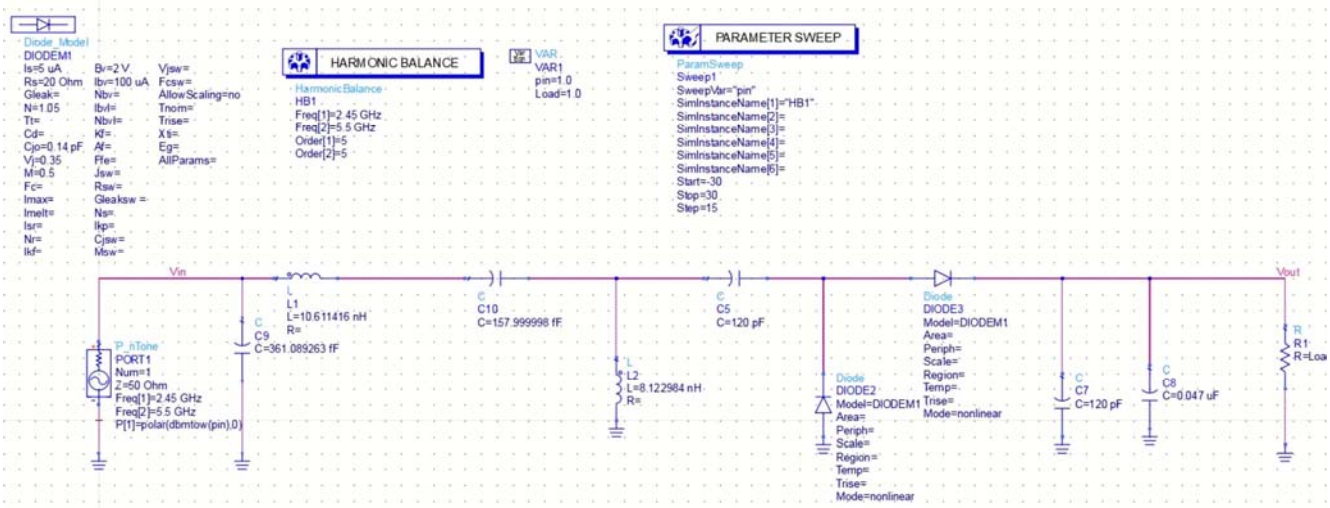

Fig. 9 Circuit design for dual-band RFEH for 2.45 GHz and 5.5 GHz

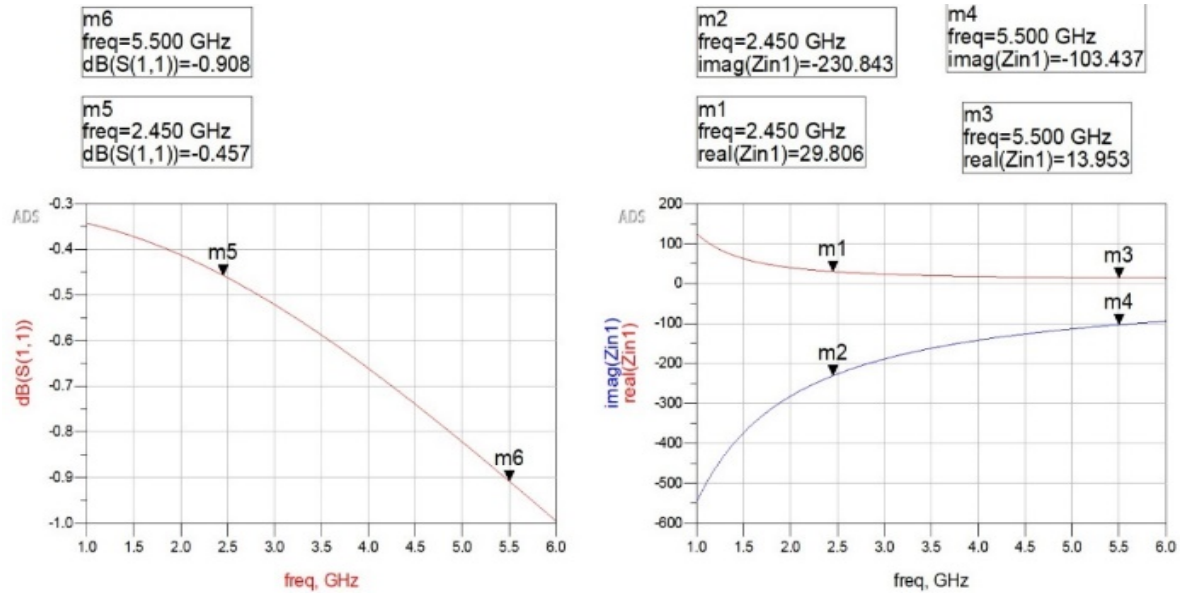

Fig. 10 The return loss coefficient and the impedance of the circuit design without IMN

Using the ADS Smith Chart Utility tool (Fig. 5), the lumped component IMN was designed to match the standard input antenna impedance (Zs = 50 Ω) with Z_L = 29.806 - j230.843 Ω at 2.45 GHz and Z_L = 13.953-j*103.437 as shown in Fig. 10. Z_L represents the real and imaginary parts of the impedance, as the VMC includes a frequency-dependent capacitor. S_{11} at 2.45 GHz is -0.457, and at 5.5 GHz is -0.908, as shown in Fig. 10.

To achieve impedance matching at 2.45 GHz and 5.5 GHz, the extracted optimized values from ADS are C1 = 361.089263pF, L1 = 10.611416 nH, C2 = 157.999998 pF and L2 8.122984 nH, respectively. With the matching network, the rectifier's equivalent impedance becomes (43.115 + j5.345 at 2.45 GHz and 49.285 + j1.554 at 5.5 GHz) Ω, which is very close to the 50 Ω input antenna port impedance. The simulated return loss coefficient (S_{11}) at the IMN input, indicates that matching at the desired frequencies has been achieved. The S_{11} is -20.588 at 2.45 GHz and -35.274 at 5.5 GHz frequencies, respectively.

Fig. 11 shows a graph of the reflection coefficient (S_{11}) vs. frequency to analyze the rectifier's return-loss performance with

and without an impedance-matching circuit. Due to the impedance matching, the return loss significantly decreases at the matching frequency. The matching network is considered satisfactory at an input power of -30 dBm.

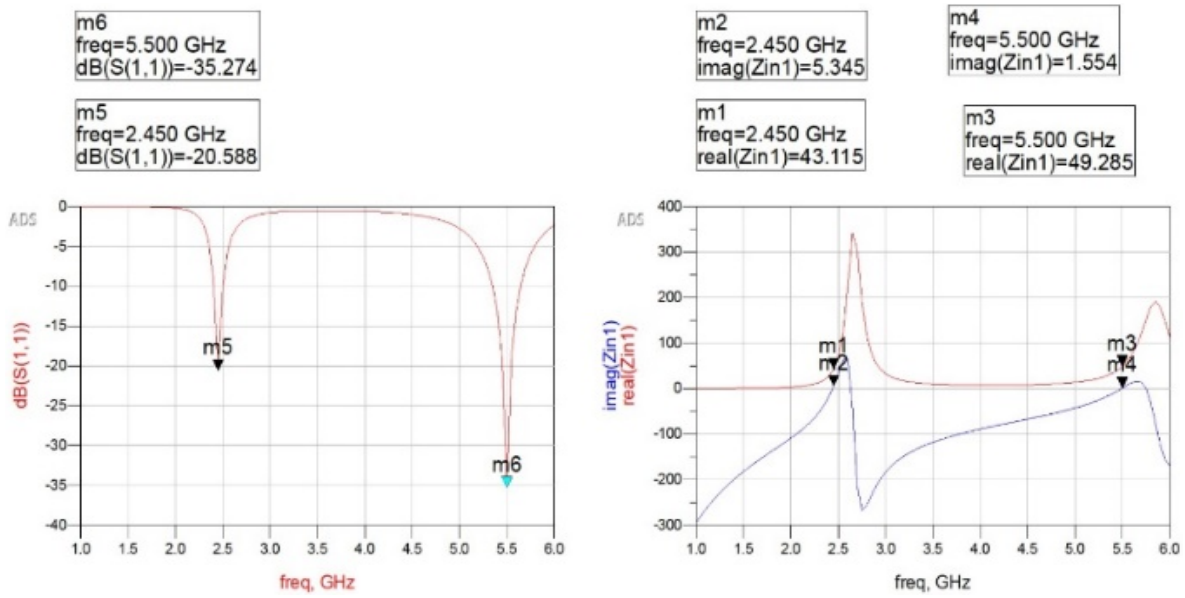

Fig. 11 The return loss coefficient and the impedance of the circuit design with IMN

III. Solar Energy Harvester

Photovoltaic cells are fabricated using various methods and materials. Despite their differences, their primary function remains to extract electrical energy from sunlight. Three leading PV cell technologies dominate the global market: monocrystalline, polycrystalline silicon, and thin film. These technologies have become industry leaders.

The solar system comprises three main parts: solar panels, an MPPT controller, and a boost converter. Solar panels extract power from sunlight using semiconducting materials. The MPPT controller improves conversion efficiency and prevents battery overcharging or unnecessary discharge. The boost converter moves the low DC harvesting voltage to a high voltage level to meet battery power demands. A solar energy harvester is designed that can produce a voltage of 9 V at the output when harvested with an input voltage of 4 V.

A. Solar Energy Harvester Design

The solar cell generates a current of 0.16 A, charging the input filter capacitor C1 and creating a voltage across it. When this voltage reaches 4 V (the comparator reference voltage (Vref = 4 V) of the MPPT circuit), the comparator activates the MOSFET transistor BSC019NE2LSI through the driver. With the transistor on, inductor L1 connects to the ground, and the input filter capacitor C1 (already charged to 4 V) begins discharging through inductor L1 to the ground. During this discharge, the inductor stores energy in its magnetic field. When the input filter capacitor C1 discharges to 4 V, the MPPT circuit comparator deactivates the transistor BSC019NE2LSI. The charged inductor then discharges to the output capacitor C2 and loads RL through the Schottky diode D. As the inductor discharges, the input capacitor charges again from the solar cells to 4V, and the process repeats.

Some assumptions were made here:

- Ignoring the effect of resistance in the inductor and capacitor of the boost converter
- Output voltage V_o = 9 V
- Frequency f = 25 KHz
- R3 = 25 kΩ
- V_H = 4.2 V
- V_L = 3.8 V

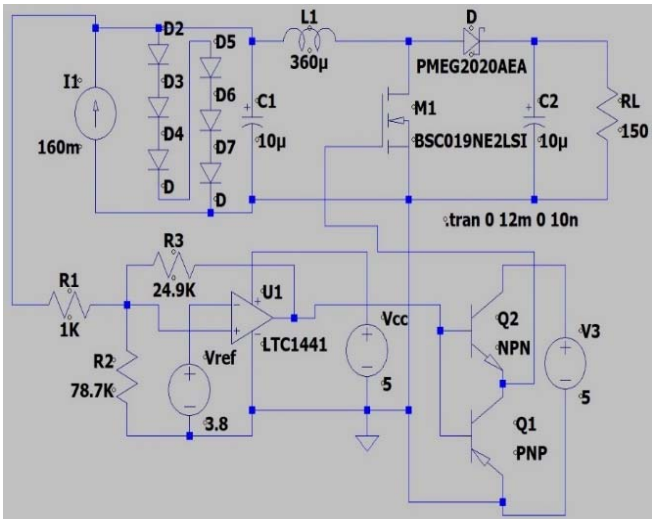

Fig. 12 Circuit design for Solar EH

- Solar Panel: The solar panel is modelled as a current source into a diode.

To calculate the number of diodes used for the solar panel:

– Expected input voltage V_S = 4 V
– Diode V_{th} = 0.7 V

$$\text{Number of diodes} = \frac{V_s}{V_{th}} = \frac{4}{0.7} = 6$$

- Boost converter

$$Time\ T = \frac{1}{f} \tag{5}$$

$$T = \frac{1}{f} = \frac{1}{25000} = 40us$$

To calculate the duty cycle *D* from [27].

$$D = 1 - \frac{V_{in}}{V_o} \tag{6}$$

$$D = 1 - \frac{V_{in}}{V_o} = 1 - \frac{4}{9} = 0.55$$

$T_{on} = DT = 40 * 0.56 = 22\ us$

$T_{off} = T - T_{on} = 40 - 22 = 18\ us$

Values of the inductor L1 and the capacitors C1 and C2 are calculated as [27]:

$$C = C1 = C2 = \frac{D}{R\frac{\Delta V_{out}}{V_{out}}f} \tag{7}$$

$$C = C1 = C2 = \frac{D}{R\frac{\Delta V_{out}}{V_{out}}f} = \frac{0.55}{150*0.01*25000} = 14\ uF$$

$$L = L1 = L_{\min} = \frac{D(1-D)^2R}{2f} \tag{8}$$

$$L_{\min} = \frac{0.55(1-0.55)^2 150}{2*25000} = 34\ uH$$

To calculate for R1, R2, and R3, the formulas are obtained from [28].

$$R_1 = R_3\left(\frac{V_{HB}}{V_{cc}}\right) \tag{9}$$

$V_{HB} = V_H - V_L = 4.0 - 3.8 = 0.2$ V

$$R_1 = 25000\left(\frac{0.2}{5}\right) = 1\ \text{k}\Omega\ \text{n}$$

$$V_H > V_{ref}\left(1 + \frac{V_{HB}}{V_{cc}}\right) \tag{10}$$

$$4 > V_{ref}\left(1 + \frac{0.2}{5}\right)$$

$$3.8V > V_{ref}$$

$$R_2 = {}^{1}\Big/\left[\left(\frac{V_H}{V_{ref}\times R_1}\right) - \left(\frac{1}{R_1}\right) - \left(\frac{1}{R_3}\right)\right] \tag{11}$$

$$R_2 = {}^{1}\Big/\left[\left(\frac{4.0}{3.8\times 1000}\right) - \left(\frac{1}{1000}\right) - \left(\frac{1}{25000}\right)\right] = 79\ \text{k}\Omega$$

IV. Simulation Results and Discussions

A. Antenna Simulation

The proposed microstrip rectangular patch antenna design was simulated using CST Evaluation software. Fig. 13 illustrates the variation of the reflection coefficient versus frequency, while Fig. 14 depicts the radiation pattern of the designed antenna. Table III presents the measurement results of the antenna operating at a frequency of 2.45 GHz. The antenna achieved a gain of 2.66 dBi (see Fig. 14). The measured return loss, shown in Fig. 13, is reduced to -29.6367 dB, with an acceptable bandwidth of 83 MHz (3.4%). The antenna's input impedance is 50 Ω.

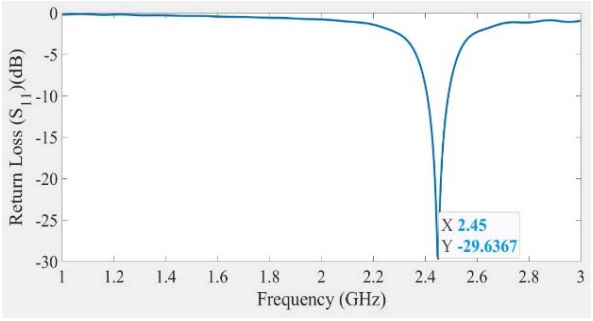

Fig. 13 Reflection coefficient vs. Frequency plot

TABLE III
Microstrip Patch Antenna Properties

Parameter	Value	Units
Gain	2.66	dBi
Return Loss (R_L)	-29.6367	Db
Input Impedance	50	Ohms
Bandwidth	83 MHz ≈ 3.4%	MHz, %

B. RF Rectifier Simulation

To simulate the output voltage for various input power levels from -30 dBm to 20 dBm, the circuit was simulated with Harmonic Balance (HB) simulation in ADS. The power intensity indicated by the antenna is represented by S_{11}, known as the reflection coefficient (or gamma). Return loss evaluates the reflected signal amount in the source, expressed in decibels (dB). A high return loss is generally desirable, as it correlates to a low insertion loss. An infinite return loss would occur if all power were transferred to the load, while no return loss would occur with an open or short circuit termination. For example, if S_{11} = 0 dB, the antenna reflects all power. For optimal S-parameters and RFEH system development, S_{11} (return loss) should be less than -10 dBm.

The IMN is a crucial subsystem in RFEH for eliminating impedance mismatch between the antenna and voltage multiplier. Additionally, the IMN increases the power gain transferred from the input antenna to the load. The simulation results in Table IV show the return loss coefficient with and without the IMN for the RFEH system at 2.45 GHz and 5.5 GHz. The IMN significantly reduced the S_{11} value to -20.588 dB and -35.274 dB, respectively, as shown in Fig. 11, compared to the case without the IMN -0.457 dB and -0.908 dB), as shown in Fig. 10. Therefore, the IMN is essential for designing the

RFEH system. Moreover, the IMN has proven to maximize the harvested power from the limited energy source. The results are given in Table VII.

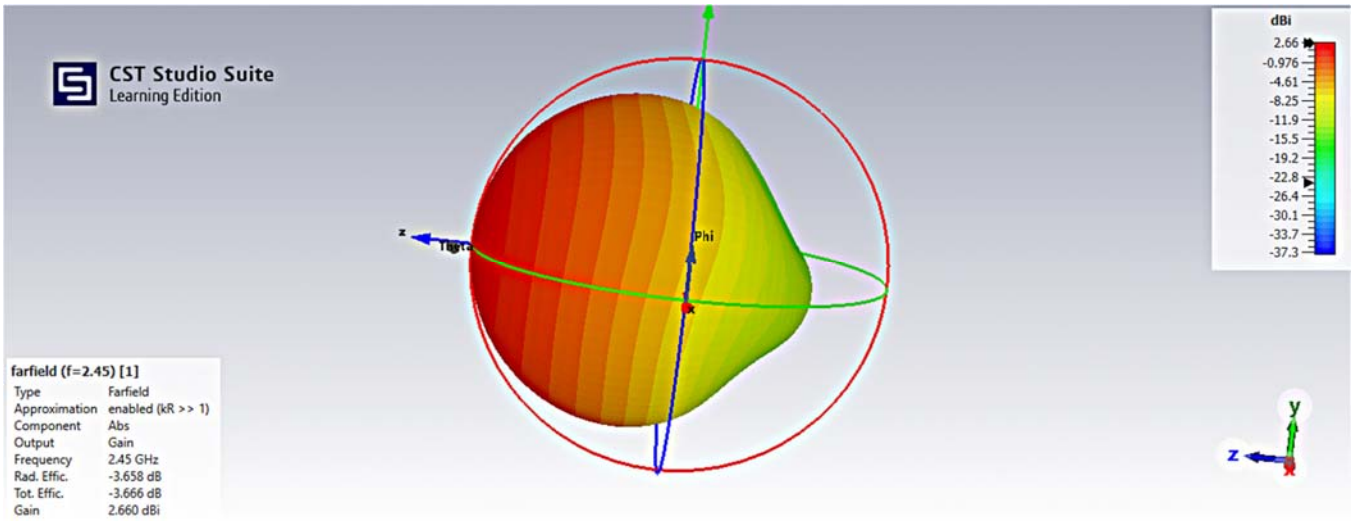

Fig. 14 Far-field radiation pattern plot

TABLE IV
RETURN LOSS COEFFICIENT (S_{11}) OF DUAL-BAND RFEH

Frequency (GHz)	S_{11} Without Matching (dB)	S_{11} With Matching (dB)
2.45	-0.457	-20.588
5.5	-0.908	-35.274

The complete RFEH system circuit in Fig. 9 was effectively simulated with the HB simulator in ADS to acquire constant DC output voltage (V_{0ut}) at various input signal power levels from -30 dBm to 30 dBm before and after the IMN was designed as shown in Figs. 15 and 16.

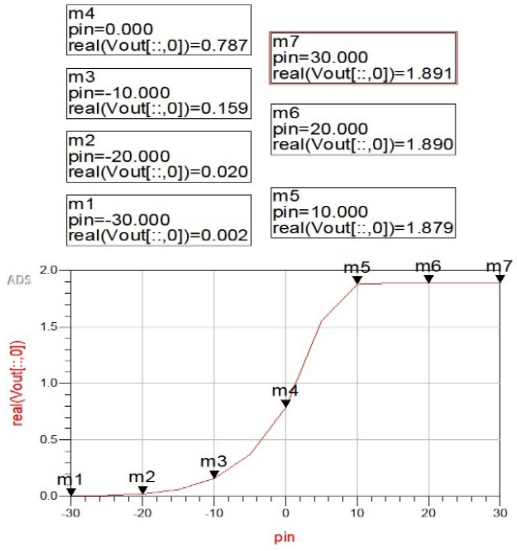

Fig. 15 V_{out} before IMN was designed for 5 kΩ

Table V demonstrates the simulated results for the constant output DC voltage for several input power signal levels.

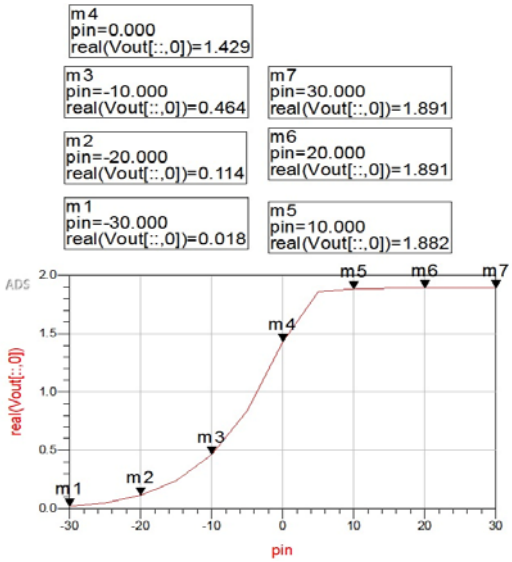

Fig. 16 V_{out} after IMN was designed for 5 kΩ

TABLE V
DC OUTPUT VOLTAGE (V_{OUT}) FOR THE DESIGNED CIRCUIT BEFORE AND AFTER IMN FOR 5 KOHM

Input Power (dBm)	Input Power (mW)	DC Output Voltage (V_{out}) Before matching network		DC Output Voltage (V_{out}) After matching network	
		2.45 GHz	5.5 GHz	2.45 GHz	5.5 GHz
-30	0.001	0.002	0.002	0.018	0.009
-20	0.01	0.020	0.020	0.114	0.071
-10	0.1	0.159	0.159	0.464	0.351
0	1	0.787	0.787	1.429	1.117
10	10	1.879	1.879	1.882	1.865
20	100	1.890	1.890	1.891	1.891
30	1000	1.891	1.891	1.891	1.891

The results show a direct proportionality between the DC output voltage and the RF input power level. As the input power

signal in the RFEH circuit system increases, the output voltage also automatically increases due to the VMC's ability to boost the low input signal. This relationship between output voltage and input power levels is clearly shown in Fig. 16. The DC output voltage is maximum when the input power equals or exceeds 5 dBm. However, the circuit can still produce a significant DC voltage for input power levels like -30 dBm.

Reference [29] gives the conversion efficiency (PCE) between RF input and DC output:

$$\eta_{\%} = \frac{P_{out}}{P_{in}} \tag{12}$$

$$P_{out} = \frac{{V_o}^2}{R_L} \tag{13}$$

where η% is the power conversion efficiency; P_{out} is the DC output power; P_{in} is the RF input power; V_0 is the DC output voltage; R_L is the output load resistance.

The power conversion efficiency (PCE) for several levels of RF input power ranging from -30 dBm to 30 dBm is calculated using (11) and (12) and presented in Table VI.

TABLE VI
SHOWING THE VALUES OF CONVERSION EFFICIENCY (PCE) FOR DIFFERENT INPUT POWER

Input Power (dBm)	Input Power (mW)	Efficiency %	
		2.45 GHz	5.5 GHz
-30	0.001	6.48	0.10
-20	0.01	25.99	10.08
-10	0.1	43.31	24.64
0	1	40.84	24.95
10	10	7.08	6.96
20	100	0.72	0.72
30	1000	0.07	0.07

The results demonstrate the highest efficiency when establishing the IMN between the source impedance and the load impedance. Furthermore, when the circuit resonates at the desired frequency, the IMN improves circuit efficiency [30]. As the input power approaches its maximum level, the efficiency gradually decreases due to the IMN's inability to handle high input signals effectively. Conversely, the IMN performs well with low input signals, primarily enhancing the antenna's weak signal before the VMC further amplifies it. Fig. 17 shows the relationship between the PCE and RF input power levels.

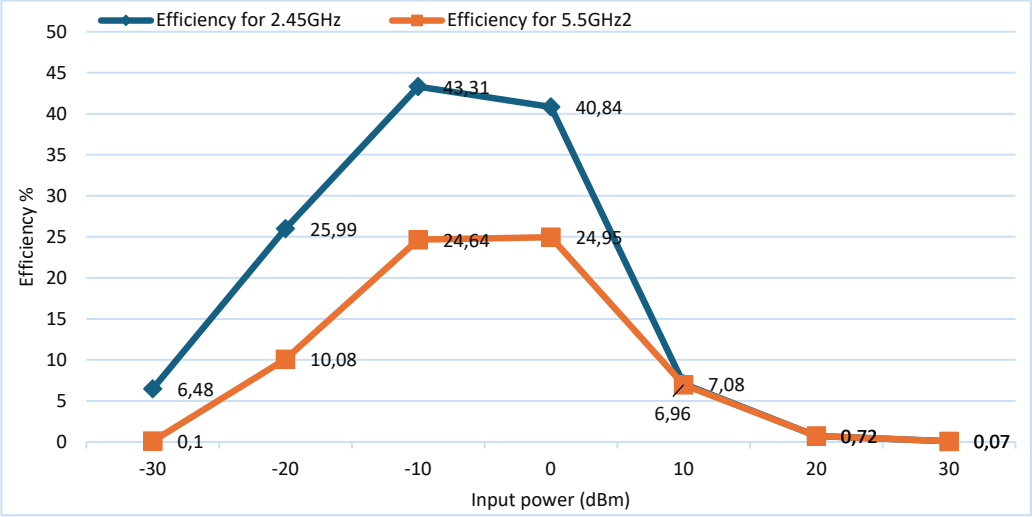

Fig. 17 Relationship between the PCE and RF input power levels

We observed that the system's efficiency dropped as the input power signal increased from 0 dBm. However, efficiency increased when the input signal power was between -30 dBm and -10 dBm, indicating that the impedance matching is well-suited for low input signal conversion. Additionally, Fig. 17 shows that at the input power of -30 dBm, the lowest efficiency was observed, while higher efficiency is achieved for higher input power levels. The highest efficiency for 2.45 GHz and 5.5 GHz bands for input powers of -10 dBm is 43.31% and 24.64%, respectively.

Table VII presents the simulated conversion efficiency of the RFEH versus input power levels at seven different output load resistances.

TABLE VII
EFFICIENCY OVER DIFFERENT LOADS

Input power (dBm)	Output load resistance (kΩ)	Efficiency
		2.45 GHz
-10	5	43.31
	10	33.99
	25	19.09
	50	10.86
	100	5.85
	500	1.27
	1000	0.64

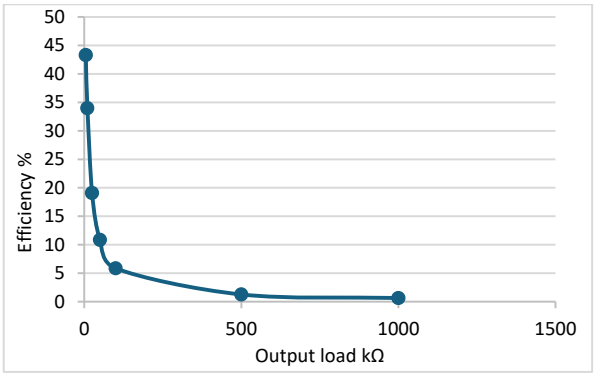

Fig. 18 Conversion efficiency over different output load

The conversion efficiency at the target output load resistance has been maintained effectively, particularly at 5 kΩ. Fig. 18 shows the simulated RF to DC conversion efficiency of the RFEH circuit system at seven respective output load values with an input power level of -10 dBm. The conversion efficiency of the RFEH circuit highly depends on the load resistance, as seen in Fig. 18. Various output load values were considered in the HB simulations, and a 5 kΩ load resistance was selected as the optimal value for WSN sensor devices.

C. Solar Energy Harvester Simulation

It is observed that $V_0 = 9$ V as wanted.

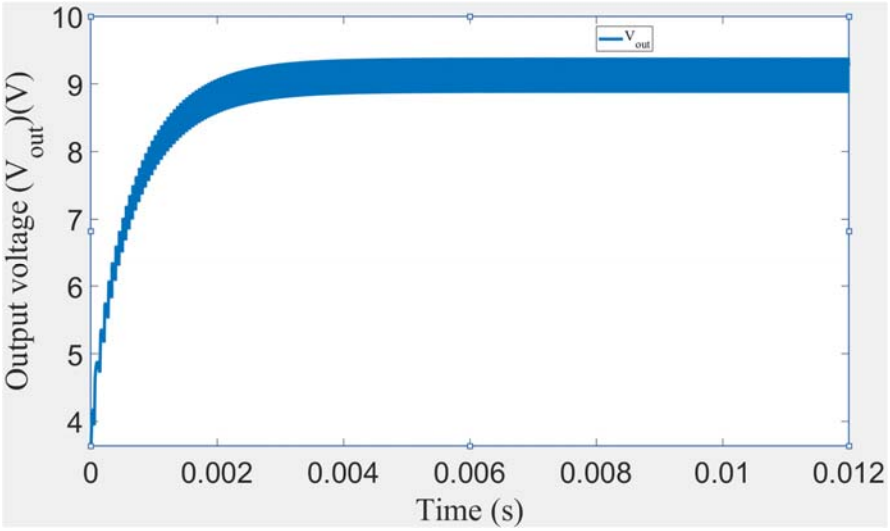

Fig. 19 Output voltage from LTspice simulator

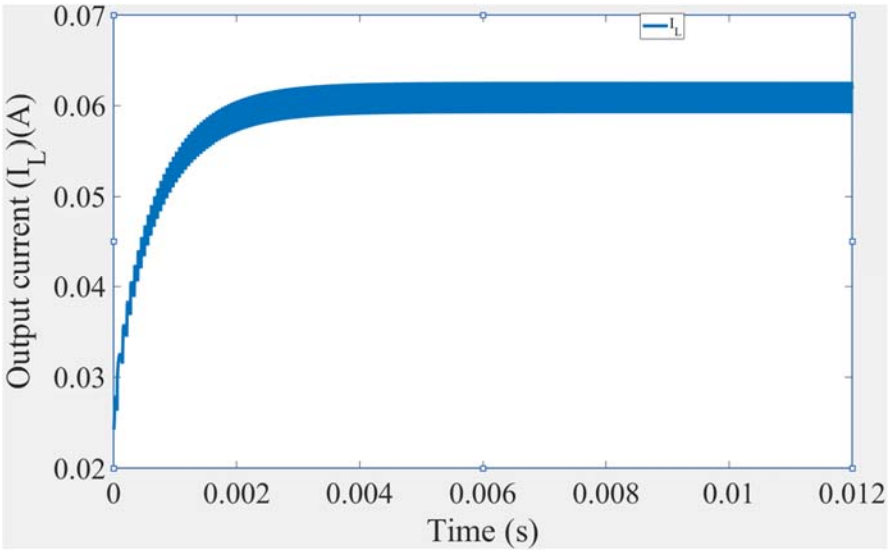

Fig. 20 Output current or Load current

From Fig. 20,

$I_L = 60$ mA

$P_{out} = V_0 * I_L = 9 * 0.06 = 0.54$ W

$P_{in} = V_s * I_s = 4 * 0.16 = 0.64$ W

$$\text{Conversion Efficiency} = \frac{P_{out}}{P_{in}} * 100\%$$

$$\frac{0.54}{0.64} * 100 = 84.375\%$$

V. Conclusion

A dual-band RFEH circuit operating at 2.45 GHz and 5.5 GHz carrier frequencies is proposed. Using Agilent ADS software, the VMC was simulated, and its performance was analyzed with and without impedance matching. IMN was established across all standard frequency bands using a microstrip stubs configuration. These simulations are crucial for optimizing the entire RFEH system.

The output DC voltage was simulated for single-tone input signals with power levels ranging from -30 dBm to 30 dBm, showing increased output voltage as input power levels rose. The RF-DC conversion efficiency was simulated over various input power levels, achieving optimal efficiency at -10 dBm with 43.31% at 2.45 GHz and 24.64% at 5.5 GHz. Notably, the proposed RFEH system can still provide adequate DC output voltage at low RF input power levels.

The return loss S11 significantly decreased to -20.588 dB at 2.45 GHz and -35.274 dB at 5.5 GHz after IMN was implemented, highlighting the importance of IMN in RFEH system design. Additionally, IMN has proven effective in maximizing harvested power from limited energy sources.

The proposed circuit is suitable for a low-power application since it may be used with a variety of battery-free WSN circuits and devices. As such, the modeling and fabrication of the RF harvester circuit rely significantly on simulation. The power of the input signal will be divided among several output ports by a power combiner/splitter circuit in later research, guaranteeing optimal input and output port matching, excellent isolation, and low loss in a narrow band. For practical design and operation in communication systems including transceivers, phased arrays, and power amplifiers, this power combiner circuit is essential.

A. Study Limitations

Variability in the Environment: Circumstances over which there is little control may impact the accuracy of outcomes.

Component Variability: Variations in a component's performance and quality can affect an experiment's results.

Scalability: The outcomes might translate poorly to more complex systems or other applications.

Future research could focus on:

- *Enhanced Modeling:* Refining models to better account for environmental and component variability.
- *Long-Term Studies:* Performing extended experiments to assess system performance over longer periods.
- *Alternative Sources:* Investigating additional energy sources and their integration into multisource systems.
- *Advanced Materials:* Investigating cutting-edge materials for adaptable and lightweight energy-harvesting components. It is critical to look into new materials and technologies in order to lower the cost and increase the efficiency of solar panels and RF harvesters.
- *Integration Techniques:* It is suggested that better techniques for combining solar and radiofrequency energy gathering devices be developed in order to enhance power management and energy storage systems. Power conversion and storage must be optimized in order to maximize system performance as a whole.

References

[1] S. Priya and D. J. Inman, Energy Harvesting Technologies, vol. 21. Springer, 2009.

[2] J. McCullagh, "An active diode full-wave charge pump for low acceleration infrastructure-based non-periodic vibration energy harvesting," IEEE Trans. Circuits Syst. I, Reg. Papers, vol. 65, no. 5, pp. 1758–1770, May 2018.

[3] F. Wei, Y. Li, Q. Sui, X. Lin, L. Chen, Z. Chen, Z. Li, "A novel thermal energy storage system in smart building based on phase change material," IEEE Trans. Smart Grid, vol. 10, no. 3, pp. 2846–2857, May 2018.

[4] C. Alippi and C. Galperti, "An adaptive system for optimal solar energy harvesting in wireless sensor network nodes," IEEE Trans. Circuits Syst. I, Reg. Papers, vol. 55, no. 6, pp. 1742–1750, Jul. 2008.

[5] W. C. Brown, "The history of power transmission by radio waves," IEEE Trans. Microw. Theory Techn., vol. MTT-32, no. 9, pp. 1230–1242, Sep. 1984.

[6] J. Bito, R. Bahr, J. G. Hester, S. A. Nauroze, A. Georgiadis, and M. M. Tentzeris, "A novel solar and electromagnetic energy harvesting system with a 3-D printed package for energy efficient Internet-ofThings wireless sensors," IEEE Trans. Microw. Theory Techn., vol. 65, no. 5, pp. 1831–1842, May 2017.

[7] J. Colomer, J. Brufau, P. Miribel, A. Saiz-Vela, M. Puig, and J. Samitier, "Novel autonomous low power VLSI system powered by ambient mechanical vibrations and solar cells for portable applications in a 0.13 µ technology," in Proc. IEEE Power Electron. Specialists Conf., Jun. 2007, pp. 2786–2791.

[8] C. Ding, N. Liu, Y. Wang, J. Li, S. Heidari, J. Hu, Y. Liu, "Multisource indoor energy harvesting for non-volatile processors," IEEE Design Test, vol. 34, no. 3, pp. 42–49, Jun. 2017.

[9] Palattella M. R., Accettura N., Vilajosana X., Watteyne T., Grieco L. A., Boggia G., Dohler M. Standardized protocol stack for the internet of (important) things. IEEE communications surveys & tutorials. 2012 Dec 12;15(3):1389-406.

[10] Aichberger C., Jungmeier G. Environmental life cycle impacts of automotive batteries based on a literature review. Energies. 2020 Dec 1;13(23):6345.

[11] Rey S. O., Romero J. A., Romero L. T., Martínez À. F., Roger X. S., Qamar M. A., Domínguez-García J. L., Gevorkov L. Powering the future: a comprehensive review of battery energy storage systems. Energies. 2023 Sep 1;16(17):6344.

[12] RoboticsBiz. Batteries for IoT: Challenges and key factors in maximizing battery life (Internet). (cited 2024 jul 9). Available from: https://roboticsbiz.com/batteries-for-iot-challenges-and-key-factors-in-maximizing-battery-life/

[13] Arshi O., Rai A., Gupta G., Pandey J. K., Mondal S. IoT in energy: a comprehensive review of technologies, applications, and future directions. Peer-to-Peer Networking and Applications. 2024 Jun 4:1-40.

[14] Puluckul P. P., Weyn M. InfiniteEn: A Multi-Source Energy Harvesting System with Load Monitoring Module for Batteryless Internet of Things. In2023 IEEE 9th World Forum on Internet of Things (WF-IoT) 2023 Oct 12 (pp. 1-8). IEEE.

[15] Lal J. D., Thankachan D. Optimization of harvesting source selection based on weighted TLbO for multisource energy harvesting networks. InAIP Conference Proceedings 2024 Feb 29 (Vol. 2942, No. 1). AIP Publishing.

[16] Sun W., Liu C., Qian M., Chen Y., Xu S. Joint spectral efficiency optimization of uplink and downlink for massive MIMO-enabled wireless energy harvesting systems. EURASIP Journal on Wireless Communications and Networking. 2021 Dec;2021:1-23.

[17] Obilikpa S., Onochie U., Nweze C., Nwoziri C., Kalu B., Anazodo K. B., Nweke C. The major mechanisms for efficient hybrid energy harvesting: overview and recent developments. Asian Review of Mechanical Engineering. 2021 Sep 21;10(2):10-23.

[18] United Nations. Renewable energy: Powering a safer future (Internet). (cited 2024 Sep 9). Available from: https://www.un.org/en/climatechange/raising-ambition/renewable-energy

[19] Deng F., Yue X., Fan X., Guan S., Xu Y., Chen J. Multisource energy harvesting system for a wireless sensor network node in the field environment. IEEE Internet of Things Journal. 2018 Aug 14;6(1):918-27.
[20] Chaour I., Fakhfakh A., Kanoun O. Patch antenna array for RF energy harvesting systems in 2.4 GHz WLAN frequency band. In2018 15th International Multi-Conference on Systems, Signals & Devices (SSD) 2018 Mar 19 (pp. 179-183). IEEE.
[21] V. Kushwah, G. Tomar, Size reduction of Microstrip Patch Antenna using Defected Microstrip Structures, International Conference on Communication Systems and Network Technologies, 2011
[22] D. M. Pozar, Microstrip Antennas, Proc. IEEE, Vol. 80, pp.79- 81, January, 1992
[23] Barman R., Shinha S., Roy S., Avishek D. Design of inset feed microstrip patch antenna for bluetooth application. Int. Res. J. Eng. Technol. 2017 Mar;4(3):2385-7.
[24] Y. Uzun, Design and implementation of RF energy harvesting system, Journal of Electronic Materials, 45, 2016, 3842- 3847.
[25] Yusoff S. S., Malik S. A., Ibrahim T. Simulation and performance analysis of a dual GSM Band rectifier circuit for ambient RF energy harvesting. Applications of Modelling and Simulation. 2021 Apr 15;5:125-33.
[26] Akanksha S. Salve, Rahul V. Misal, Ganesh M. Kale, S. B Deosark and S. L. Nalbalwar, Analysis of circular microstrip antenna using different substrates for bluetooth application, International Research Journal of Engineering and Technology, 6(4), 2019, 3540-3543.
[27] Tran H. T., Nguyen M. T., Nguyen C. V., Ala G., Viola F., Colak I. Hybrid solar-RF energy harvesting mechanisms for remote sensing devices. International Journal of Renewable Energy Research (IJRER). 2022 Mar 31;12(1):294-304.
[28] Hart D. W., Hart D. W. Power electronics. New York: McGraw-Hill; 2011 Feb.
[29] Parna Kundu (datta), Juin Acharjee and Kaushik Mandal, Design of an efficient rectifier circuit for RF energy harvesting system, International Journal of Advanced Engineering and Management, 2(4), 2017, 94-97
[30] Al-Azawy M. M., Sari F. Analysis of Dickson voltage multiplier for RF energy harvesting. In2019 1st Global Power, Energy and Communication Conference (GPECOM) 2019 Jun 12 (pp. 10-14). IEEE.